Electronic Supporting Information

Photoluminescence and Electroluminescence Characterization of High Performance Near-Infrared Emitters Based on 1,5-Naphthyridin-4-ol Containing Heteroleptic Platinum (II) Complexes

Hagos Tesfay Kidanu,[abc] Jian Haur Lee[abc] and Chin-Ti Chen*[a]

[a] Institute of Chemistry, Academia Sinica, Taipei 11529, Taiwan, Republic of China.
   Email: chintchen@gate.sinica.edu.tw; Fax: +886 2 27831237; Tel: + 886 2 55728542.
[b] Sustainable Chemical Science and Technology (SCST), Taiwan International Graduate
   Program (TIGP), Academia Sinica, Taipei 11529, Taiwan, Republic of China.
[c] Department of Applied Chemistry, National Yang Ming Chiao Tung University, Hsinchu
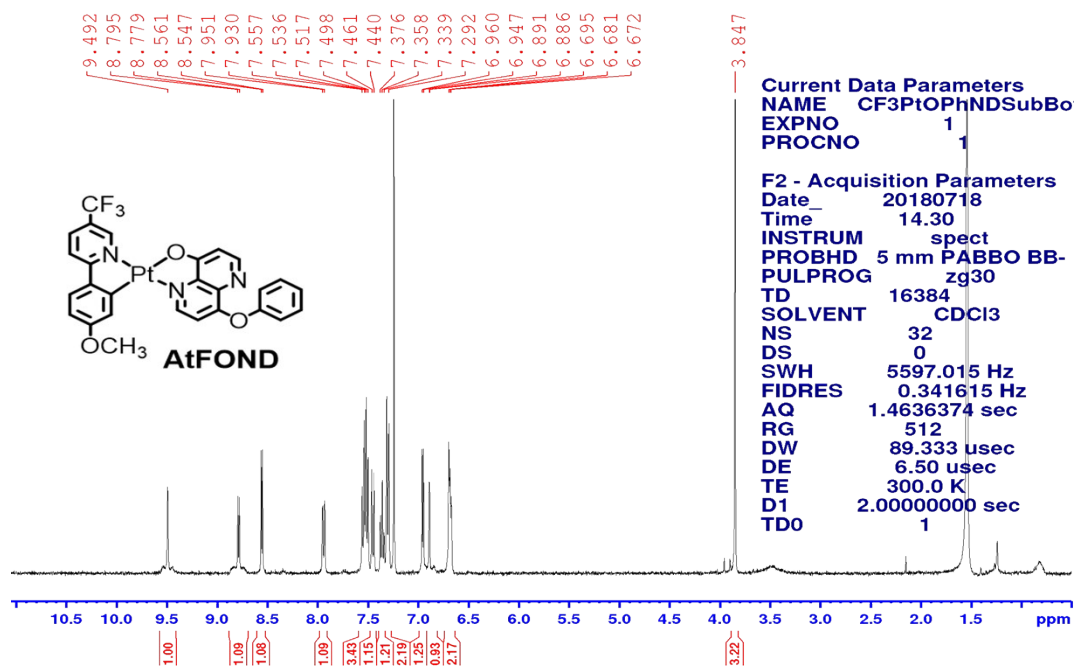   30050, Taiwan, Republic of China.

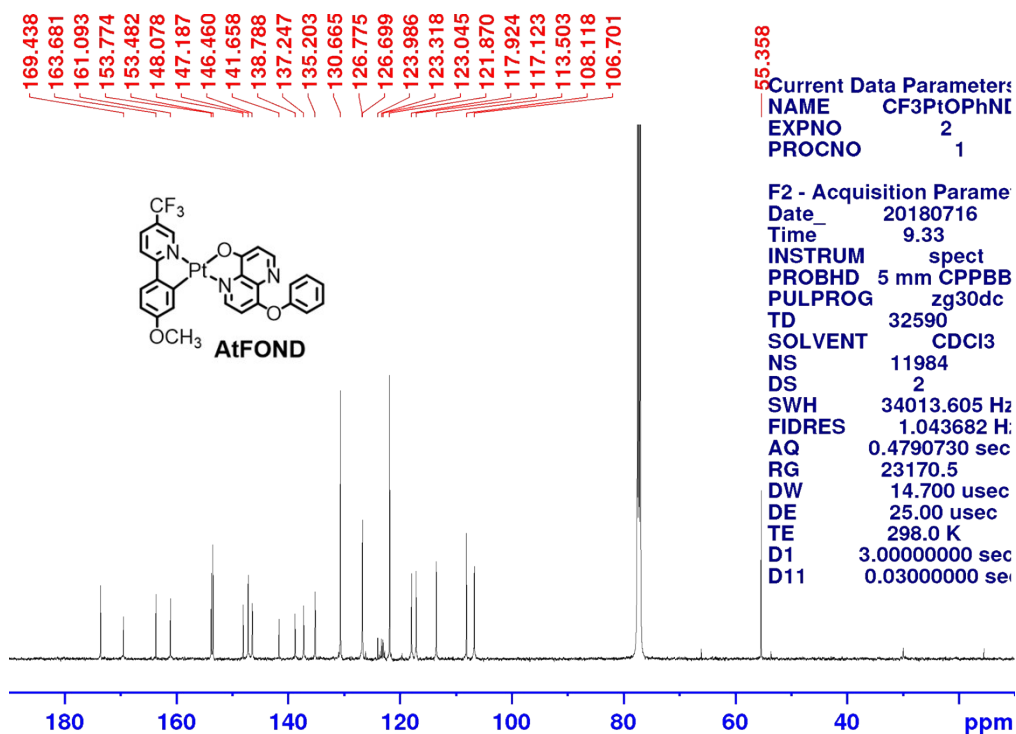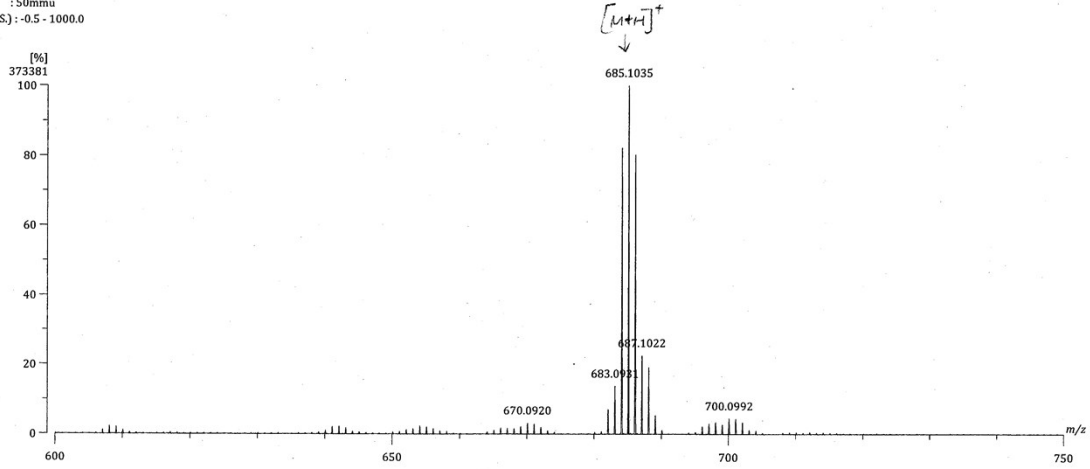**Figure S1**. ^{1}H NMR spectrum of **AtFOND** (400 MHz, CDCl$_3$).

Figure S2. ^{13}C NMR spectrum of **AtFOND** (125 MHz, CDCl$_3$).

trans-AtFOND (HR-FAB)

$[M+H]^+$

685.1035

687.1022

683.0931

670.0920

700.0992

m/z

Observed m/z   Int%   Err[ppm / mmu]   U.S. Composition
1   685.1035   100.00   +1.3 / +0.9   18.5   C27 H19 F3 N3 O3 Pt   = 685.1026

Figure S3. HR-MS spectrum of **AtFOND**.

$[M-Cl]^+$

700.2

Exact Mass: 735.0687

$[M+H]^+$

736.2

341.5

447.1

607.6

matrix NBA
307.3
359.4
391.4
483.1
579.6
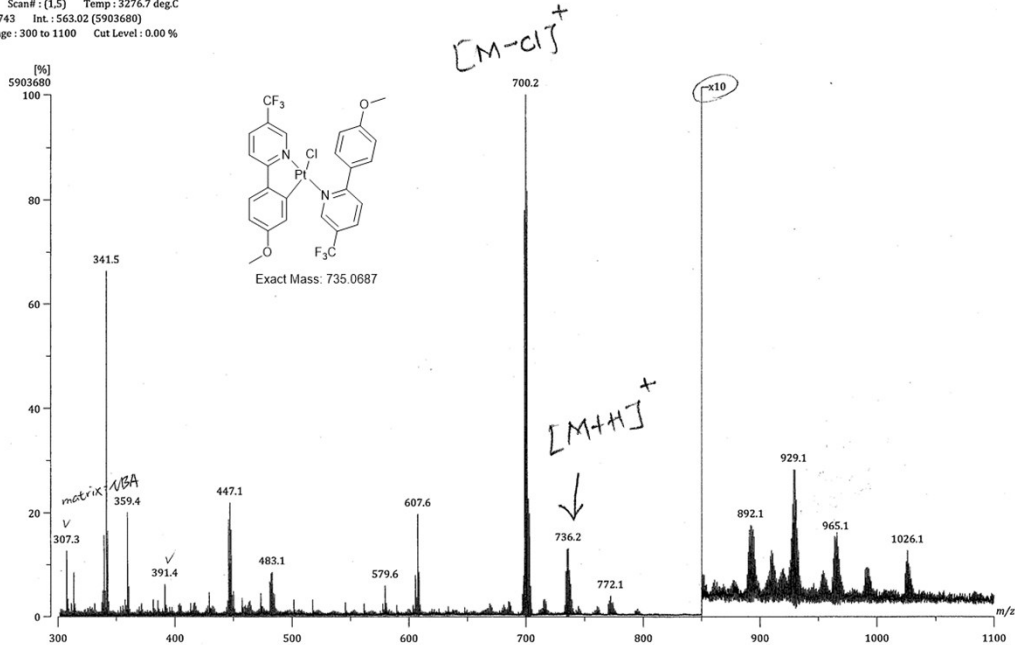772.1

×10

929.1
892.1
965.1
1026.1

m/z

Figure S4. FAB-MS spectrum of **(AtF)₂PtCl**.
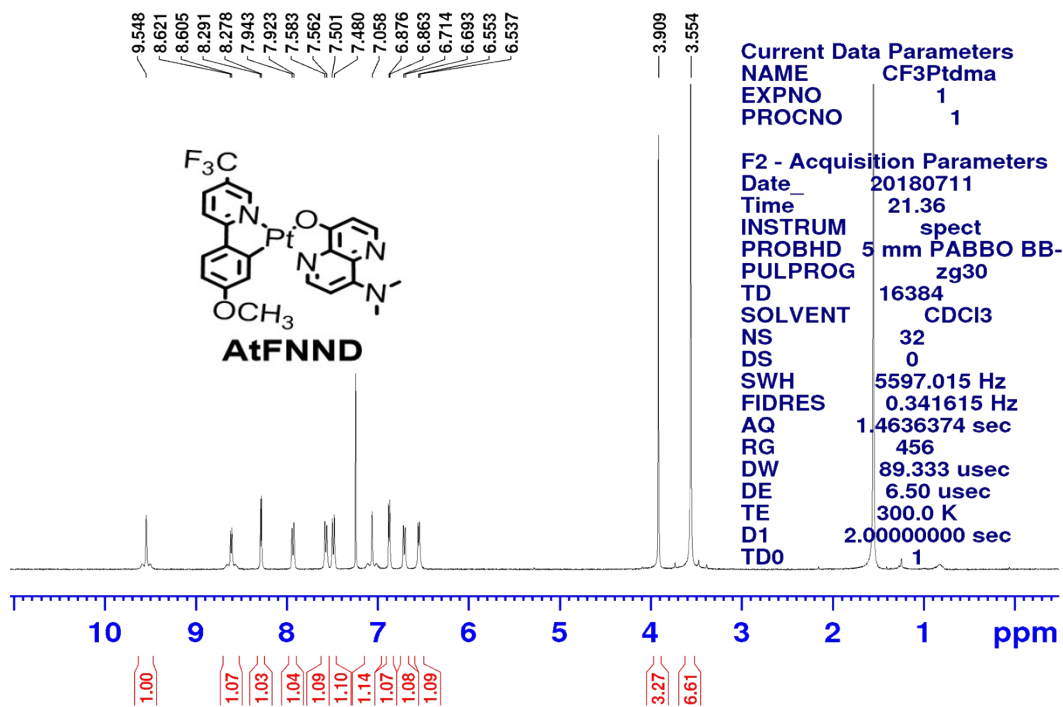
Figure S5. 1H NMR spectrum of **AtFNND** (400 MHz, CDCl3).
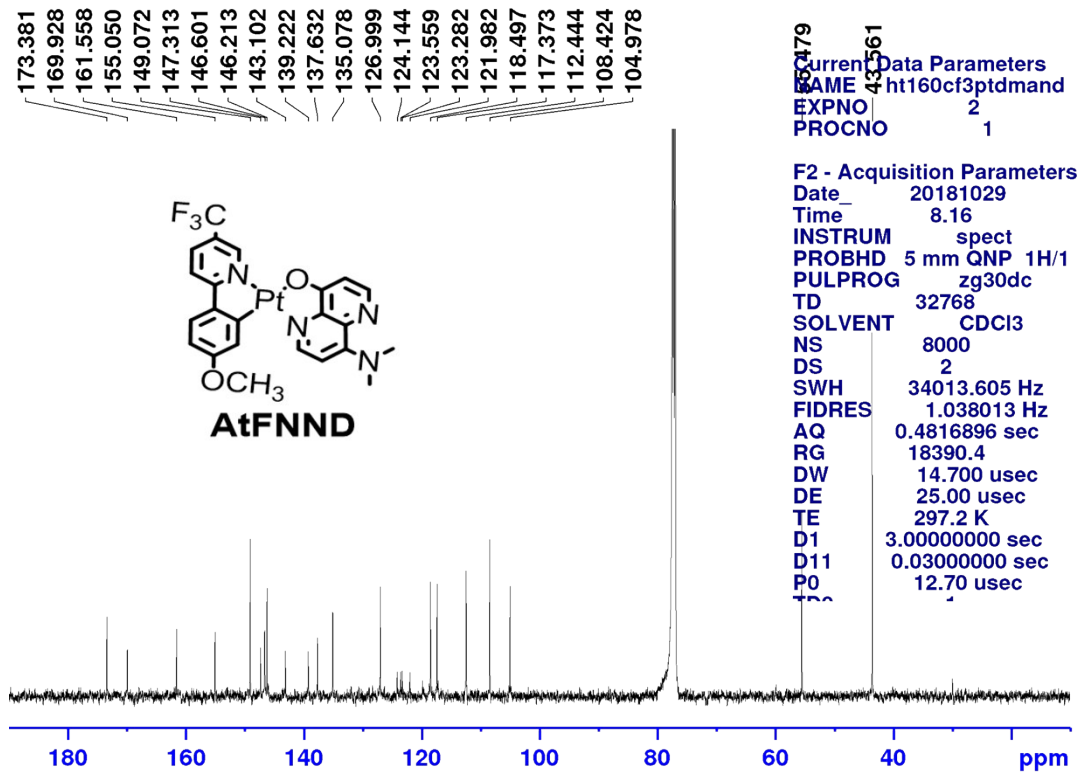
Figure S6. ^{13}C NMR spectrum of **AtFNND** (125 MHz, CDCl$_3$).

Figure S7. HR-MS spectrum of **AtFNND**.

Figure S8. ^{1}H NMR spectrum of **PBSOND** (400 MHz, CDCl$_3$).
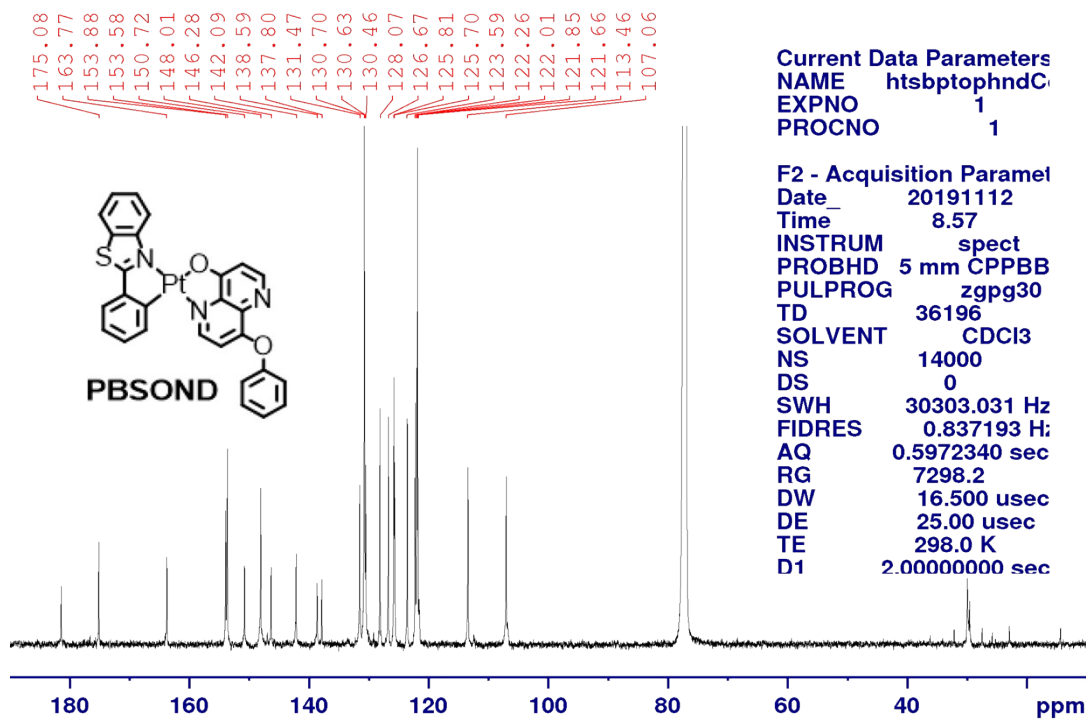
Figure S9. ^{13}C NMR spectrum of **PBSOND** (125 MHz, CDCl$_3$).
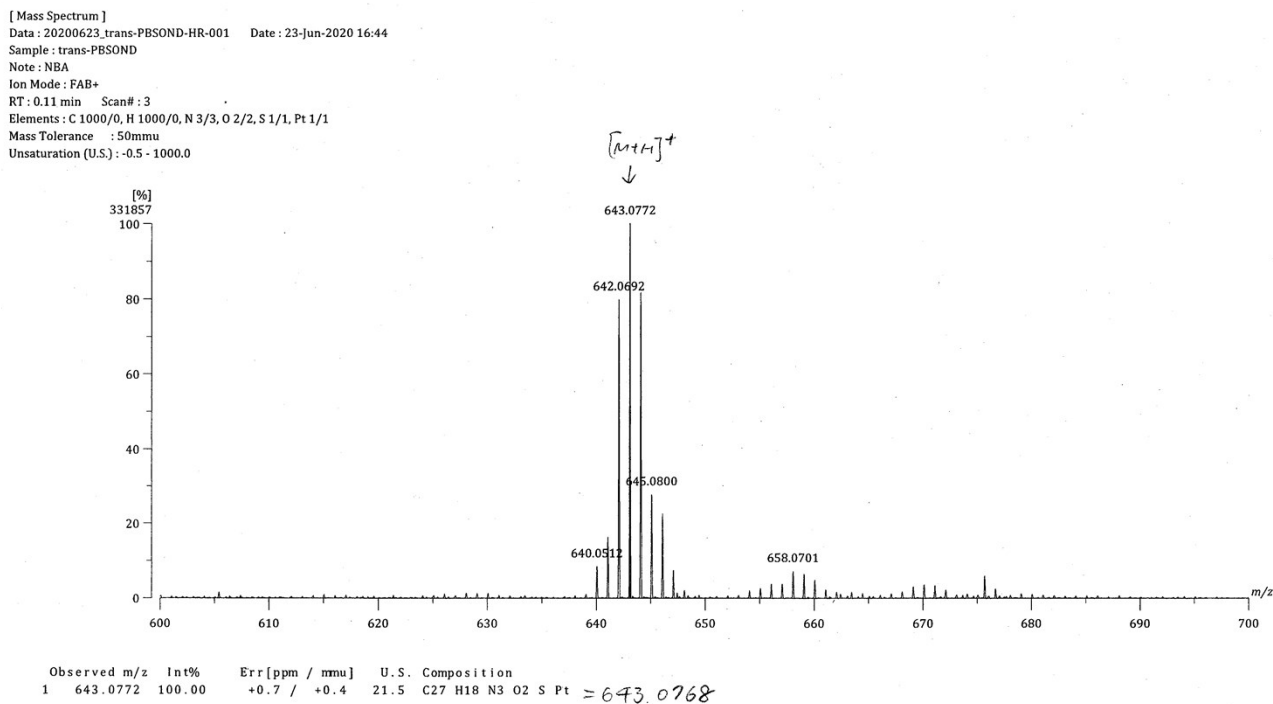
Figure S10. HR-MS spectrum of **PBSOND**.

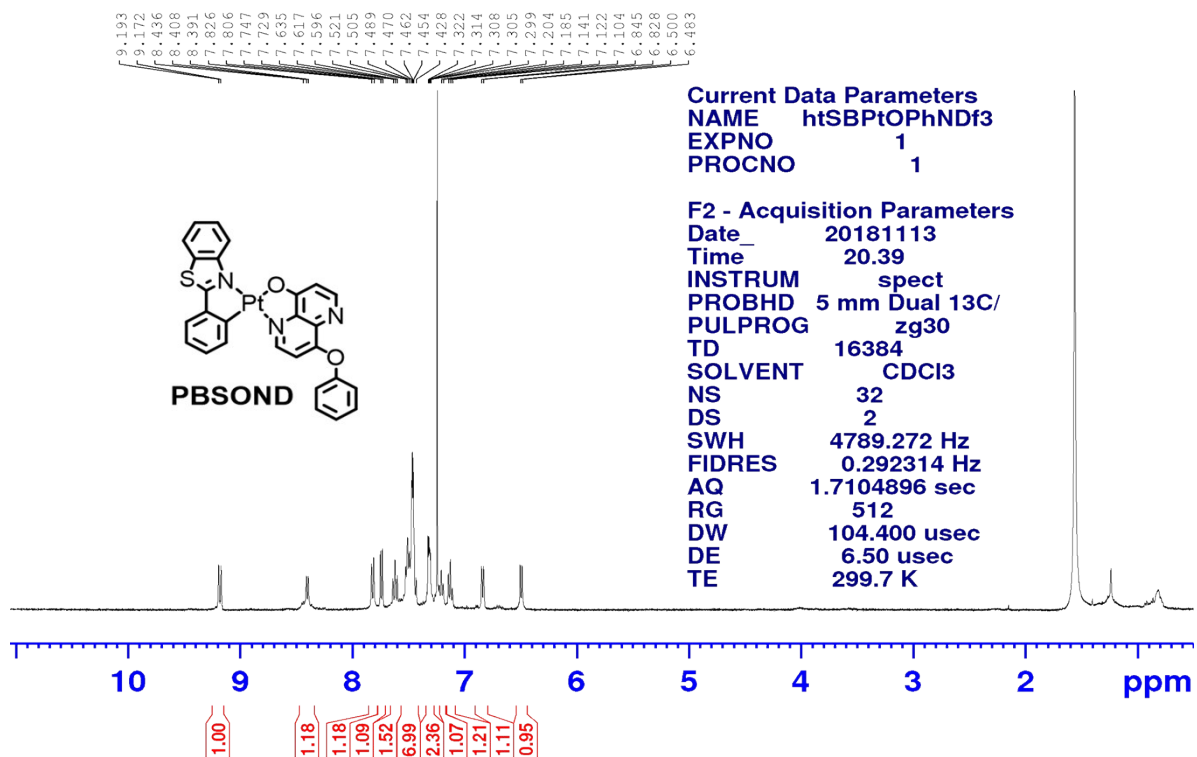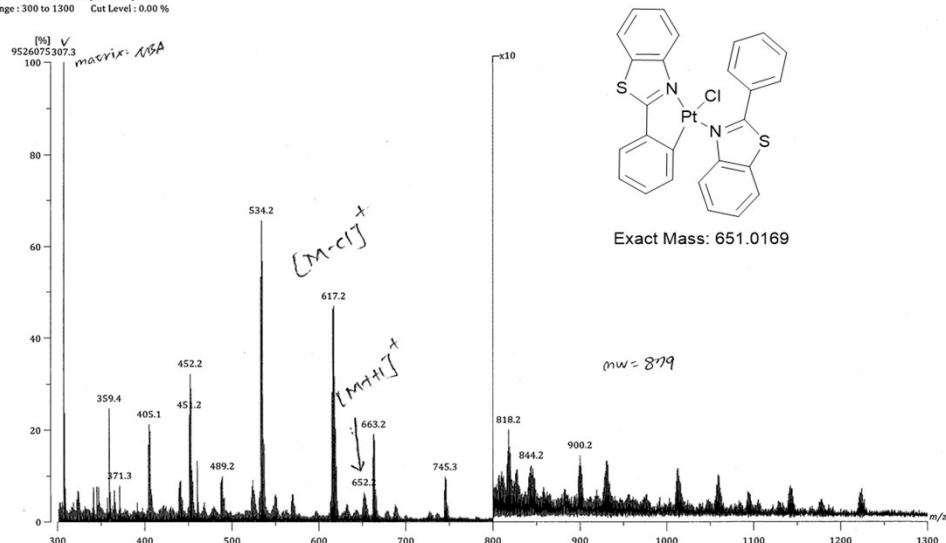**Figure S11.** FAB-MS spectrum of **(PBS)₂PtCl**.
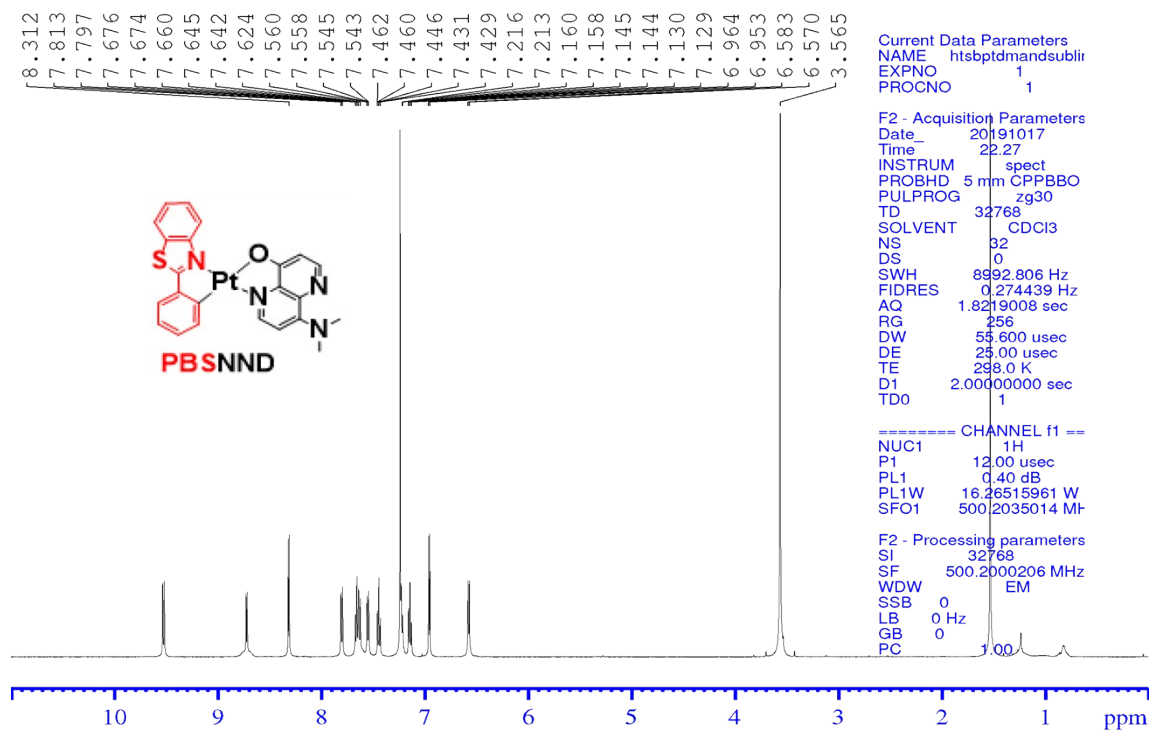
Figure S12. ¹H NMR spectrum of **PBSNND** (400 MHz, CDCl₃).
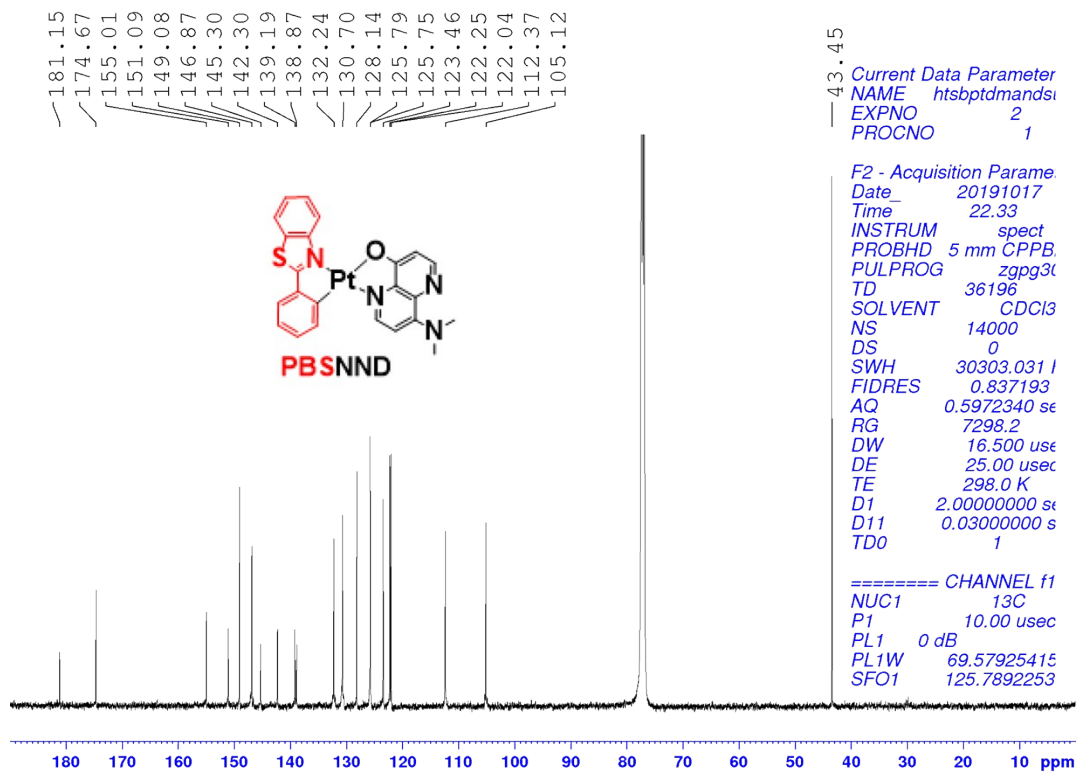
Figure S13. ^{13}C NMR spectrum of **PBSNND** (125 MHz, CDCl$_3$).

Figure S14. HR-MS spectrum of **PBSNND**.

Table S1. Comparison of selected geometric parameters of the studied platinum complexes.

Pt complexes		Selected bond lengths (Å)			
		Pt-N(1)	Pt-C	Pt-O	Pt-N(qn)
AtFOND	Crystal[a]	1.99	1.98	2.09	2.04
	DFT[b]	2.03	2.01	2.14	2.07
AtFNND	Crystal[a]	2.00	2.00	2.08	2.03
	DFT[b]	2.03	2.02	2.13	2.07
PBSOND	DFT[b]	2.06	2.02	2.15	2.07
PBSNND	Crystal[a]	2.02	1.99	2.10	2.01
	DFT[b]	2.06	2.02	2.15	2.06

Pt complexes		Selected bond angles (°)					
		O-Pt-N(1)	C-Pt-N(1)	C-Pt-N(qn)	O-Pt-N(qn)	N(1)-Pt-N(qn)	O-Pt-C
AtFOND	Crystal[a]	92.7	81.0	105.3	81.1	173.6	172.1
	DFT[b]	93.6	80.5	106.6	79.6	171.6	172.7
AtFNND	Crystal[a]	92.1	81.2	106.1	80.6	171.7	173.2
	DFT[b]	93.6	80.6	106.8	79.3	171.8	173.1
PBSOND	DFT[b]	97.9	80.1	103.6	79.0	173.2	173.8
PBSNND	Crystal[a]	97.8	80.8	101.8	80.5	173.4	172.4
	DFT[b]	98.1	80.0	103.8	78.8	173.3	173.9

[a] Results obtained experimentally from the single crystal X-ray structure. [b] Results obtained by DFT calculation using b3lyp method for the ground state geometry .
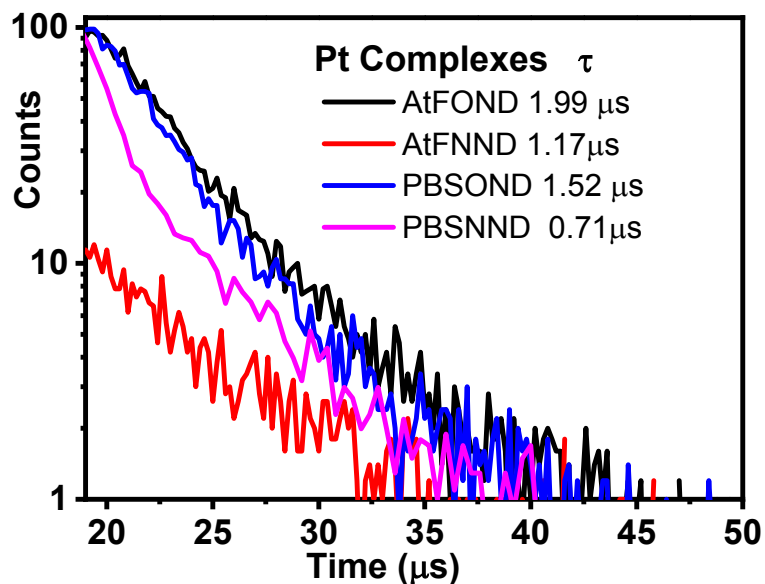
Figure S15. Decay profile of the PL intensity of studied platinum complexes in degassed CH_2Cl_2 at room temperatures.

AtFOND

AtFNND

PBSNND

Figure S16. Molecular interaction in the crystal of **AtFOND** (top), **AtFNND** (center), and **PBSNND** (bottom).

Theoretical studies

All of the calculations were performed with the Gaussian 16 program package. The geometry optimization of ground states of the studied Pt(II) complexes were simulated with DFT at the B3LYP/LANL2DZ (Pt) and B3LYP/ 6-31g(d,p) (H, C, N, S, O) levels using CH_2Cl_2 as the solvent. The optimized structures of **AtFOND**, **AtFNND**, **PBSOND** and **PBSNND** complexes were used to calculate the 12 lowest singlet ($S_0 \rightarrow S_{12}$) and triplet optical electronic transitions ($S_0 \rightarrow T_{12}$) using the TD-DFT method. The solvent effect is based on the polarizable continuum model (PCM), which is implemented in the Gaussian 16 program. The contribution of a group to a molecular orbital was calculated within the framework of Mulliken population analysis using the AOMix program. The calculated optical absorption and emission transition characters of all the complexes in dichloromethane are summarized in Table S2. While the frontier molecular orbitals involved in the lower-lying transitions are depicted in Fig. 4.

Table S2. Calculated wavelengths and molecular orbitals character of the optical transitions for the studied platinum complexes in dichloromethane solvent

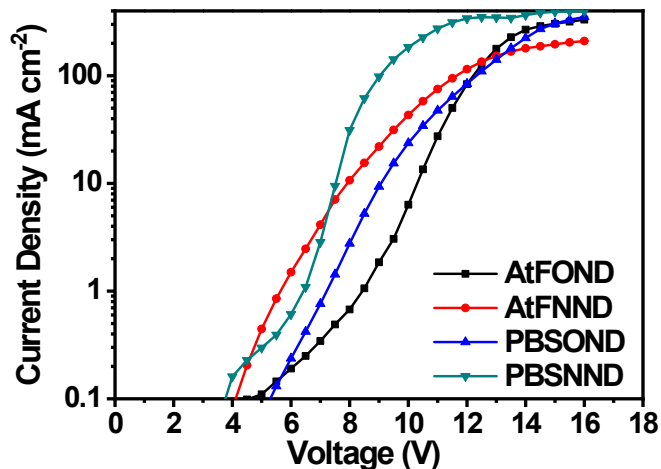| Complex	State	λ (nm)	Main contribution of MOs (%)
AtFOND	$S_0 \rightarrow S_1$	432	HOMO $\rightarrow$ LUMO (69)
	$S_0 \rightarrow T_1$	507	HOMO $\rightarrow$ LUMO (61)
AtFNND	$S_0 \rightarrow S_1$	454	HOMO $\rightarrow$ LUMO (67)
	$S_0 \rightarrow T_1$	505	HOMO $\rightarrow$ LUMO (49)
PBSOND	$S_0 \rightarrow S_1$	435	HOMO $\rightarrow$ LUMO (68)
	$S_0 \rightarrow T_1$	519	HOMO $\rightarrow$ LUMO (56)
PBSNND	$S_0 \rightarrow S_1$	438	HOMO $\rightarrow$ LUMO (66)
	$S_0 \rightarrow T_1$	508	HOMO $\rightarrow$ LUMO (40)

Fig. S17. The current density and voltage characteristics of four NIR platinum complex OLEDs.
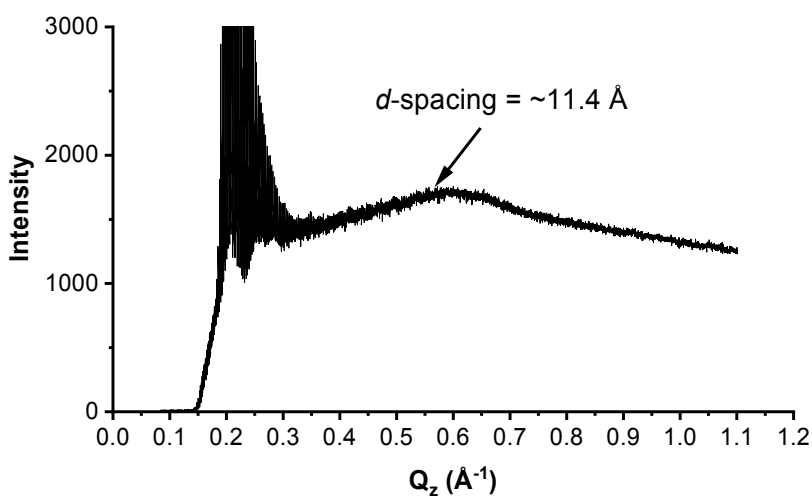

Figure S18. 1D GIWAXS spectrum of **PBSNND** along the direction of Q_z (out-of-plane direction to the substrate) extracted from the corresponding 2D GIWAXS patterns (Fig. 10). The corresponding d-spacing, $d = 2\pi/Q_z$.